

# Peculiarities in quantification of airborne particulate matter by means of Total Reflection X-ray Fluorescence

Yves Kayser,<sup>\*,†</sup> János Osán,<sup>‡</sup> Philipp Hönicke,<sup>†</sup> and Burkhard Beckhoff<sup>†</sup>

<sup>†</sup>*Physikalisch-Technische Bundesanstalt, Abbestraße 2-12, 10587 Berlin, Germany*

<sup>‡</sup>*Environmental Physics Department, Centre for Energy Research, Konkoly-Thege M. út  
29-33., 1121 Budapest, Hungary*

E-mail: yves.kayser@ptb.de

## Abstract

Knowledge on the temporal and size distribution of particulate matter (PM) in air as well as on its elemental composition is a key information for source appointment, for the investigation of their influence on environmental processes and for providing valid data for climate models. A prerequisite is that size fractionated sampling times of few hours must be achieved such that anthropogenic and natural emissions can be correctly identified. While cascade impactors allow for time- and size-resolved collection of airborne PM, total reflection X-ray fluorescence (TXRF) allows for element-sensitive investigation of low sample amounts thanks to its detection sensitivity. However, during quantification by means of TXRF it is crucial to be aware of the limits of TXRF in order to identify situations where collection times or pollution levels were exceedingly long or high. It will be shown by means of grazing incidence X-ray fluorescence (GIXRF), where different reflection conditions are probed, that a self consistent quantification of elemental mass depositions can be performed in order to validate or identify issues in

quantification by means of TXRF. Furthermore, monitors of validity for a reliable quantification of the elemental composition of PM by means of TXRF will be introduced. The methodological approach presented can be transferred to tabletop instrumentation in order to guarantee a reliable quantification on an element sensitive basis of the PM collected. This aspect is highly relevant for defining appropriate legislation and measures for health and climate protection and for supporting their enforcement and monitoring.

## Introduction

Aerosols present in the environment affect our daily life at multiple levels. For example, airborne particulate matter (PM) in air can impact health due to inhalation<sup>1-3</sup> or can influence atmospheric processes,<sup>4</sup> more precisely the climate and environmental ecosystems through influencing cloud formation<sup>5</sup> or reflecting and scattering sunlight.<sup>6</sup> The chemical composition, which requires element-sensitive analytical methods, as well as the chemical speciation of the PM is of interest for a correct comprehension of the physical and chemical properties of the individual particles.<sup>7</sup> With regard to health concerns, the smallest particles, so called fine and ultrafine particles with sizes in the sub-micrometer and sub-100 nanometer range, are the most concerning for epidemiology as they can penetrate into the airways of the lungs and may be held responsible for health-averse effects on the respiratory and cardio-vascular system upon long-term exposure.<sup>8-11</sup> In particular anthropogenic emissions result in a noticeably higher generation of ultrafine particles.<sup>12</sup> While toxicological studies have to assess possible health risks of different nanomaterials,<sup>13</sup> parallel efforts have to be undertaken to quantify the presence of the different elements in air and consider their dilution under different weather conditions, at best in a time-resolved and size-fractionated fashion. This information is relevant for accurate modeling of climate changes, for regulatory bodies to impose preventive measures and for legal entities to enforce regulations on air quality and to correctly pinpoint anthropogenic or natural sources. Adding to this the requirement to

not only detect but to quantify reliably trace levels of aerosols contained in air in order to achieve good time resolution during environmental monitoring campaigns, highly sensitive and accurate techniques need to be used.

Among different available techniques<sup>14,15</sup> X-ray fluorescence (XRF) based methods have emerged as a promising contributor to the field by delivering ensemble information on the chemical composition. In contrast to other analytical techniques, XRF based investigations can be performed without imposing sample consumption or altering the chemical composition, which makes cross-validation measurements of other techniques feasible, and without requiring high sample concentration.<sup>14,16</sup> In combination with impactors, where the particulate matter is collected in a time- and size-resolved manner, all relevant information for quantifying the mass of different elements in a defined volume of air, even at in the range of few  $\text{ng}/\text{m}^3$ , are at hand<sup>17,18</sup> and can be applied to a wide range of elements and particle sizes.<sup>19-23</sup> Synchrotron radiation-based approaches<sup>17,18,24</sup> and total reflection XRF (TXRF)<sup>21,22,25-27</sup> were used to achieve the best possible detection limits.

It will be shown hereafter that for elemental mass depositions above trace level contamination, which can occur when sampling airborne PM without further knowledge on the air pollution levels, quantification by means of TXRF needs verification. Since TXRF is a single-point measurement technique, cross-validation and indicators are required to identify when quantification could be compromised. Grazing incidence X-ray fluorescence (GIXRF) and X-ray reflectivity (XRR) will be used since these techniques are able to deliver information beyond the horizon of TXRF. Indeed, during a GIXRF measurement the incidence angle is varied such that the excitation conditions are varied from excitation under total reflection conditions to excitation under shallow incidence angle. Using this information, GIXRF allows for a robust assessment of the validity of quantification under TXRF conditions and for self consistent quantification where quantification by means of TXRF is comprised by to high mass deposition of airborne PM. Furthermore, XRR will be introduced as a monitor of the validity of TXRF quantification results.

## Quantification by means of TXRF

TXRF employs a specific geometry in which the X-ray beam used for the excitation of the XRF signal impinges the sample at a very shallow angle beneath the critical angle for total external reflection.<sup>28</sup> Hence, TXRF demands for collimated and monochromatic excitation conditions but offers advantages such as the illumination of large sample areas and a large solid angle of detection. Further benefits offered by TXRF are twofold. On the one side, the penetration of the incident beam into the substrate is reduced to an evanescent wave and any background signal, XRF or scattering, originating from it is suppressed. On the other side, the reflection of the incident X-ray beam at the substrate surface leads to the creation of a X-ray standing wavefield (XSW) due to interference between incident and reflected X-rays. Consequently, enhanced excitation conditions for XRF originating from the particulate matter deposited on the top of the substrate can be achieved. A prerequisite to profit from total external reflection is to use substrates which are flat on a macroscopic scale and characterized on a microscopic scale by a roughness smaller than the wavelength of the incident X-rays.

The knowledge of the XSW is of importance for quantitative measurements independently if external standardization, internal standardization or reference-free quantification schemes are applied. When using internal standardization the XSW created needs to be identical throughout the sample area illuminated, while in case of external standardization the same XSW needs to be created in a reproducible manner for all samples investigated. External standardization means that for each element of interest in an experimental campaign a calibration curve is established by means of a set of reference samples with different mass depositions of the selected elements. This approach requires adequate reference samples which are sufficiently representative of the samples investigated.<sup>29,30</sup> For samples collected during outdoor campaigns the criteria include elemental composition (sample matrix), mass deposition (concentration), particle size range and morphology as well as deposition pattern. Hence, the production and selection of adequate calibration samples for outdoor sampling

campaigns requires additional a priori information. The characterization of actual samples from the measurement campaign via complementary techniques in order to use these samples as a kind of standards is often impeded by the sensitivity, i.e., the amount of sample required, of these techniques.

For this reason approaches based on internal standardization were developed as an alternative that can be used with digested samples or in conjunction with substrates prepared for sampling.<sup>18,31</sup> Internal standardization means that on each sample to be analyzed a known quantity of a reference element is added beforehand of the measurement while assuming that the excitation and detection conditions at the position where the standard is deposited is representative for the whole sample. However, the standard which is added needs to fulfill the requirements of non-toxicity, not being ubiquitous and having XRF energies which do not overlap with the XRF lines to be contained within the sample. The goal of both approaches, external and internal standardization, is to extract combined information on instrumental factors in order to allow quantifying the elemental content of the material deposited on the top of the substrates.

In the reference-free XRF quantification scheme,<sup>25</sup> information on the different experimental and fundamental parameters is used to calculate the mass deposition of different elements from the measured count rate of the corresponding fluorescence line. This approach requires the use of (radiometrically) calibrated instrumentation, e.g. apertures, diodes and silicon drift detector (SDD) for an accurate knowledge of the solid angle of detection, the incident photon flux and the detected XRF intensity, and the knowledge of atomic fundamental parameters (FPs), such as ionization cross-sections and fluorescence factors, which are element-dependent and in a large part also energy-dependent, is also required.

## Samples

The size-fractionated sampling of PM was realized by means of a 9-stage extension of the May-type cascade impactor.<sup>32</sup> The aerodynamic cut-off diameters of the stages 1 to 9 are respectively 17.9  $\mu\text{m}$ , 8.9  $\mu\text{m}$ , 4.5  $\mu\text{m}$ , 2.25  $\mu\text{m}$ , 1.13  $\mu\text{m}$ , 0.57  $\mu\text{m}$ , 0.29  $\mu\text{m}$ , 0.18  $\mu\text{m}$  and 0.07  $\mu\text{m}$ . The cut-off diameter is defined as the dimension of the PM which is collected with 50% efficiency, smaller particles escaping with a higher probability. A well-known and constant airflow is required during the collection of airborne PM. The first two stages with the coarsest particle sizes were disregarded and for the 7 further stages  $20 \times 20 \text{ mm}^2$  Si wafers are used as substrates. As Si wafers have very low background contamination and very low surface roughness, they are ideally suited for TXRF and GIXRF experiments. Measurements with good signal-to-background ratio can be expected even though other substrates might be more suitable for the collection of PM. Indeed, the collection efficiency depends not only on the design of the airflow, where losses of particles should be minimized,<sup>33</sup> but also on the substrate surface which can be pre-treated to minimize bounce-off effects for example. This requires, however, additional a posteriori treatment prior TXRF investigation<sup>21</sup> and is detrimental if other, complementary analytical techniques shall be used as well. Hence, in order to preserve the capabilities offered by TXRF, no pre-treatment was used. Sample sets selected for the present study were collected from two campaigns at two cities, Budapest, Hungary, 24 – 31 May 2018; and Cassino, Central Italy, 20–27 September 2018, with sampling duration ranging from 20 min to 5 h. In total 19 Si substrates collected on the 3 stages with the finest particle distributions were used in this survey. More information on 6 of these 19 samples is provided in Table 1.

The deposition area from the May-type cascade impactor corresponds to a stripe of 20 mm length and, depending on the stage, of 0.1 to 1 mm width (fine to coarser PM). The width is determined by the width of the slits used as nozzles for the different stages. This type of deposition pattern presents the advantage of being highly suitable for investigation by means of TXRF and GIXRF once the stripe is aligned along the incidence direction. Thus, the

May-type cascade impactor is ideal to demonstrate the capability offered by the combination of cascade impactors and TXRF, respectively GIXRF analysis to provide element, size- and time-resolved information on the PM collected.

Table 1: Description of the 6 selected Si substrates with aerosol particles collected in Budapest and at Cassino which are discussed in more details in Figure 2 and 3. Samples are listed in the order of deposited particulate mass and cover the full range of elemental mass depositions quantified on the total of 19 samples investigated.

Sample	Duration	Stage	Diameter range / nm
A	30 min	7	300 – 600
B	20 min	9	70 – 180
C	20 min	8	180 – 300
D	1 h	7	300 – 600
E	5 h	9	70 – 180
F	5 h	7	300 – 600

## Experimental

The reference-free GIXRF measurements<sup>25,34,35</sup> for quantification of elemental mass depositions present in the particulate matter collected were realized at the plane grating monochromator (PGM)<sup>36</sup> beamline in the PTB laboratory at the BESSY II electron storage ring. The experiments were conducted at an incident photon energy of 1620 eV which is below the Si K-edge in order to suppress the contribution of the Si K XRF lines. An ultrahigh-vacuum chamber equipped with a 9-axis manipulator was used.<sup>37</sup> The instrument allows for precisely tuning the incident angle  $\theta$  between the incidence direction of the synchrotron radiation and the sample surface (Fig. 1). The fluorescence radiation emitted from the sample was detected by means of a silicon drift detector (SDD) calibrated in terms of response function<sup>38</sup> and detection efficiency,<sup>39</sup> which is placed in the polarization plane and perpendicular to the propagation direction of the linearly polarized incident X-ray beam in order to minimize scattered radiation. The SDD allows for an energy-dispersive detection of the XRF emitted from the sample such that the information from different elements can be discriminated

and processed in parallel during quantification. The incident photon flux is determined by using a calibrated photodiode. The spectra were deconvoluted using the known detector response functions for the relevant fluorescence lines and background contributions, which was mainly resonant Raman scattering (RRS) from the Si K shell<sup>40</sup> and to a lower extent Bremsstrahlung from L shell electrons from the Si substrate. The resulting count rate  $I$  for each fluorescence line of interest is normalized with respect to the sine of the incident angle  $\theta$ , the incident photon flux  $I_0$ , the effective solid angle of detection  $\frac{\Omega}{4\pi}$  and the energy dependent detection efficiency  $\epsilon(E)$  of the SDD for the respective fluorescence photons in order to derive the emitted fluorescence intensity. It has to be emphasized that the calculation of the incident angle dependent solid angle of detection requires an accurate knowledge of the detection geometry but also of the incident beam profile.

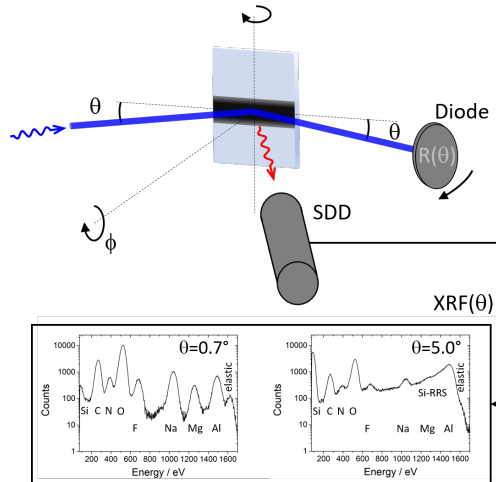


Figure 1: Illustration of the experimental setup with the Si wafer and the collected airborne PM on the top of it, a diode for measuring the reflectivity and a calibrated SDD for recording the XRF emitted for different incidence angles  $\theta$  (top panel). Typical XRF spectra recorded for an incidence angle beneath and above the critical angle of total external reflection illustrate the lower background contributions from the Si wafer at the smaller incidence angle (bottom panels).

From the absolute XRF intensity the elemental mass deposition  $m$  can be extracted for each position of the GIXRF measurements where the incident angle  $\theta$  was varied in variable steps from  $0^\circ$  to  $10^\circ$  (Figure 2). Hence, the measurement conditions on each sample were

modified from excitation under grazing incidence conditions, where an XSW needs to be considered, to excitation under shallow incidence angles, where no XSW is present. The calculation of the XSW requires the knowledge of the optical properties of the substrate for the incident photon energy used during the experiment. However, even if the incident photon energy dependent optical properties are measured beforehand from a blank Si substrate to not rely on tabulated data, the presence of the PM on the top of the Si wafer will impact the reflectivity to a certain extent as the contrast in electronic density at the interface separating the bulk Si from the vacuum or PM is changing.<sup>41</sup> Therefore, the reflectivity  $R(\theta)$  for each wafer was measured by means of a photodiode positioned in a  $\theta - 2\theta$  configuration during the GIXRF measurement. This approach allows for a direct calculation of the incident angle dependent XSW for each sample.

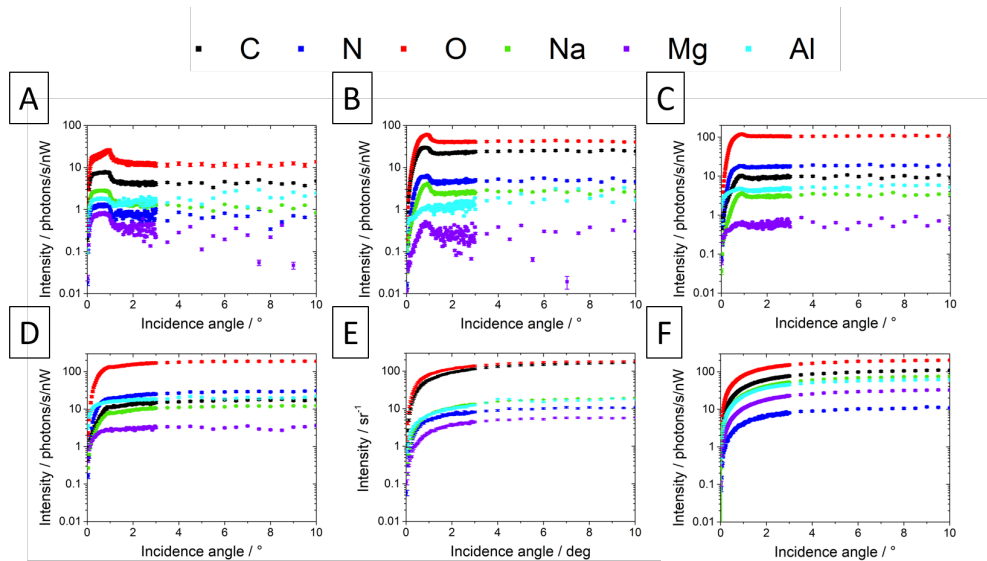


Figure 2: GIXRF data for the 6 selected different samples (labelled A to F and described in Table 1). The changes in the angular intensity profiles for each element indicate differences in the excitation of the XRF signal. The typical particle-like signature of the main elements detected in the GIXRF measurement gradually vanishes which is a clear indicator that the XSW on the top of the substrates significantly differs between the samples. It can be noted as well that for sample A, the angular evolution of O contains both particle- and layer-like signatures. The latter contribution arises from the surface oxide of the Si wafers used, but the relative contribution vanishes with increasing mass of collected airborne PM.

## Reference-free GIXRF Quantification

In a TXRF measurement the XRF intensity is usually recorded at a single incidence angle corresponding to  $\frac{1}{\sqrt{2}}$  ( $\approx 70\%$ ) of the critical angle for total external reflection  $\theta_c$ , which depends on the incident photon energy and the substrate density<sup>28</sup> and which was about  $1^\circ$  for the Si wafers used. The relative intensity distribution within the XSW is given by,<sup>28</sup>

$$XSW(\theta, z) = 1 + R(\theta) + 2\sqrt{R(\theta)} \cos \left( \arccos(2\frac{\theta^2}{\theta_c^2} - 1) - 4\pi \sin \theta \frac{z E_0}{hc} \right) \quad (1)$$

with  $E_0$  the energy of incident photons,  $z$  the height above the reflecting substrate and  $R(\theta)$  the measured reflectivity. For experimental reasons the reflectivity could only be accurately measured for incidence angles above  $0.6^\circ$ . In the following the mean intensity of the XSW, labelled  $\overline{XSW}(\theta)$ , over the direction vertical  $z$  (Figure 1) to the substrate surface is considered. The assumptions of a laterally and vertically homogeneous chemical composition of the collected PM and of PM dimensions extending over several periods  $\frac{hc}{2 E_0 \sin \theta}$  of the XSW are made thereby. The averaging of the XSW by integration is further backed up by the fact that different particles sizes and compositions are intermixed on each stage and that the deposition pattern is homogeneous along the direction of the incident radiation (Supp. Fig. 1). A more intricate calculation would require knowledge on the particle size and relative particle size distribution,<sup>42</sup> as well as on the surface coverage.<sup>41</sup> Under TXRF conditions, the mass deposition  $m_k$  of element  $k$  for each incidence angle  $\theta$  can then be determined from the respective measured XRF count rate<sup>25</sup>

$$m_k = \frac{-1}{\mu_{eff}(E_0, E_k)} \ln \left( 1 - \frac{I_k(\theta) \sin \theta \mu_{eff}(E_0, E_k)}{\frac{\Omega}{4\pi} I_0 \overline{XSW}(\theta) \omega_k \tau_k(E_0) \epsilon(E_k)} \right) \quad (2)$$

where  $\omega_k$  corresponds to the fluorescence factor and  $\tau_k(E_0)$  to the photoionization cross-section of the element being quantified. The values of atomic fundamental parameters can be found in literature databases<sup>43</sup> or selected parameters are determined in dedicated ex-

periments as for the fluorescence yield for C<sup>44</sup> or O.<sup>45</sup> The factor  $\mu_{eff}(E_0, E_k)$  accounts for the effective absorption cross-section of incident and emitted X-ray photons labelled  $\mu_{in}(E_0)$  and  $\mu_{out}(E_k)$  respectively, within the PM investigated

$$\mu_{eff}(E_0, E_k) = \sum_j c_j \left( \frac{\mu_{in,j}(E_0)}{\sin \theta} + \frac{\mu_{out,j}(E_k)}{\sin \frac{\pi}{2} - \theta} \right) \quad (3)$$

and requires hence knowledge on the mass deposition of the different elements present in order to take correctly into account the relative contributions via the factor  $c_k = \frac{\overline{m}_k}{\sum_j \overline{m}_j}$  with  $\overline{m}_k$  being the mean quantified mass deposition for element  $k$  at incidence angles above the critical angle for total external reflection (more precisely from 6° to 10°) where no XSW is present ( $\overline{XSW}(\theta) = 1$  for  $\theta > 3\theta_c$ ).

A consideration which is usually made at larger incidence angles during the quantification is the correction for absorption of X-rays on the incidence and emission paths

$$M_k(E_0, E_k) = \frac{\sum_j \overline{m}_j \left( \frac{\mu_{in,j}(E_0)}{\sin \theta} + \frac{\mu_{out,j}(E_k)}{\sin \frac{\pi}{2} - \theta} \right)}{1 - \exp\left(-\sum_j \overline{m}_j \left( \frac{\mu_{in,j}(E_0)}{\sin \theta} + \frac{\mu_{out,j}(E_k)}{\sin \frac{\pi}{2} - \theta} \right)\right)} \quad (4)$$

It was found that for incidence angles in the range from 6° to 10° this factor accounts for at most a few percent only (< 5%) for most of the samples. Only for samples with very high mass depositions a relative correction of 25% to 30% was introduced in this iterative correction scheme. For a most accurate correction factor and quantification a complete knowledge of the matrix composition is required. For the investigated samples, minor contributions of Fe and Cu were detected as well. However, Fe showed a rather layer-like angular intensity profile, such that a contamination of the substrate from a different source than airborne PM must be assumed and Cu was too low in mass deposition to allow for a reliable quantification. Furthermore, secondary fluorescence due to photoelectrons or fluorescence is neglected. This introduces only a minor error for low mass depositions but, depending on the matrix composition, should not be disregarded for high mass depositions where errors of up to 20%-30%

can be introduced.<sup>46</sup>

Finally, the GIXRF measurement allows to compare the quantification results of the elemental mass deposition  $m_k$  between TXRF conditions and XRF conditions under shallow incidence angles. The uncertainty made in the quantification depends on the uncertainties on the incident flux (1%), the XSW factor (5%) the atomic fundamental parameters (fluorescence yield, 10% for light elements, and photoionization cross-section, 7.5%), the detector efficiency and spectral deconvolution (2.5%), the counting statistics and the solid angle of detection (about 15% for the smallest incidence angles to about 4% for the largest incidence angles used for quantification).<sup>25</sup>

Note, that the mass deposition in terms of mass (or likewise number of atoms) for each element per unit area is quantified. A conversion to mass, which is a more commonly used metric in the aerosol community, can be straightforwardly realized if the area on which the airborne PM is collected and its lateral distribution are known.

## Results & Discussion

Given the uniform distribution of the PM, quantification results by means of Eq. 2 can be expect to be constant for a GIXRF measurement on a given sample. Indeed, the incidence angle should only affect the lowest limit of detection achievable but not impact the quantification result.

However, the quantification result for each sample and each element under TXRF conditions ( $\theta \approx 0.7^\circ$ ) and under XRF conditions ( $\theta > 61 + x.0^\circ$ ), only part of the samples present a good agreement (Fig. 3). The horizontal bar indicates the average mass deposition quantified at the largest incidence angles used and the vertical bar the incidence angle at which a TXRF quantification is typically performed for Si wafers and the incident photon energy used. For the lowest mass depositions used, the quantification results are independent of the incidence angle and agree reasonably well with each other (Fig. 3, upper panels). A

specificity can be observed for samples A and B where an imperfect deconvolution of the XRF spectra recorded at larger incidence angles affects the quantification results because of the underlying Si-RRS which is not perfectly described by the model used. In particular for Al, whose main characteristic line is close to the high energy cut-off of the Si RRS at 1520 eV, this results as well in a larger scattering of the quantification results at larger incidence angles. This illustrates perfectly the main benefit of TXRF for low mass depositions since it allows suppressing background contributions from the substrate.

For higher mass depositions, a discrepancy between the quantified mass depositions appears (Fig. 3, lower panels) in the sense that the under TXRF conditions the mass depositions are underestimated. This deviation occurs despite the fact that the XSW is calculated on the basis of reflectivity measured in parallel to the XRF intensity. In Fig. 4 it is shown that the reflectivity at a typical angle used for TXRF measurements drops significantly with increasing mass deposition of airborne PM. This observation means that the XSW is significantly different for each sample and different compared to the case of a blank substrate (Supp. Fig. 2). By not taking into account the how increasing mass deposition affects the contrast in optical density at the interface defined by the surface of the substrate the discrepancy between quantification results for the different incidence angles used would even be more important. This insight emphasizes the benefit of monitoring in parallel to a TXRF or GIXRF measurement the reflectivity from the sample. The dependence of the XSW on the surface coverage must to be taken into account when quantifying the mass deposition, a statement which is not only valid when using the reference-free quantification approach but also when applying an internal or external standard.

The relationship between the mass deposition and the XSW is noteworthy (Eq. 2) with regard to the need for using representative specimen, besides applying comparable experimental conditions, when applying external standards for quantification purposes. In case of internal standards, reliable results are only obtained if the collected mass deposition of the airborne PM is within the range of mass depositions covered by the standard under

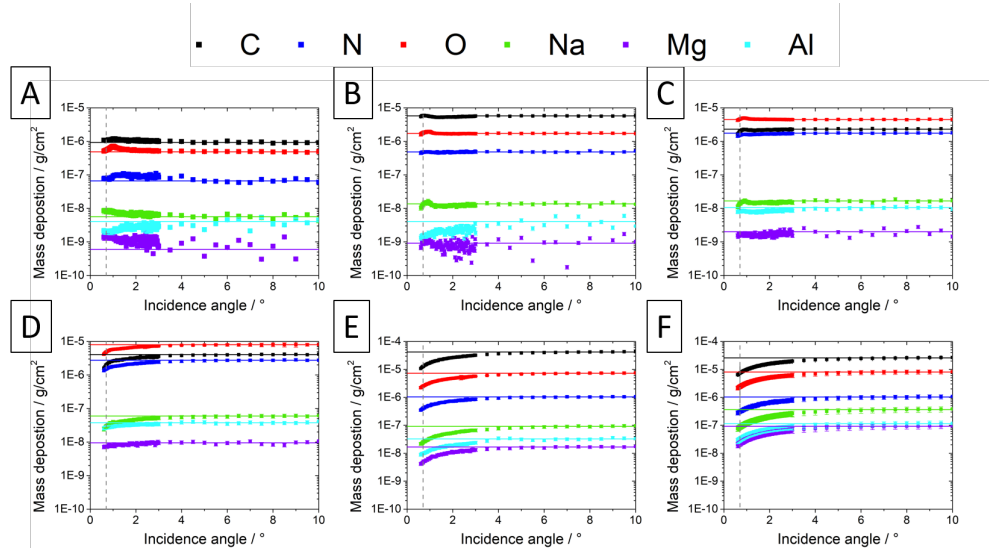


Figure 3: Quantified mass deposition for the different incidence angles covered when varying the excitation conditions during the GIXRF measurement from the TXRF regime to the XRF regime under shallow incidence angles. The vertical bar indicates the position typically selected for a TXRF measurement for a Si substrate and the incident photon energy used, while the horizontal bar indicate the mass deposition quantified at the largest incidence angles for each element. For low mass depositions (upper 3 panels) a satisfyingly good agreement can be observed, but for increasing mass deposition a growing discrepancy appears for all the elements. This indicates that not all physical effects due to attenuation of X-rays in the collected airborne PM are accounted for in the quantification scheme. Under shallow incidence angles attenuation is less important and has therefore a lesser impact on the quantification scheme as can be seen from the results approaching a constant value.

the premise that a homogeneous intermixing is realized. In other words, the dynamic range within which the calibration is valid needs to be considered. Finally, in the reference-based approaches the XSW needs to be comparable between the calibration material and investigated sample material, be it locally when using an internal standard or between samples when using an external standard, in order to avoid a calibration bias. An upper limit for reliable TXRF quantification is discussed in literature in terms of critical thickness<sup>47</sup> and saturation effect.<sup>48</sup>

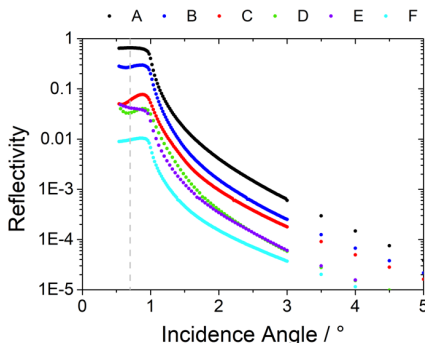


Figure 4: The reflectivity from the Si substrate for the same samples than displayed in Figures 2 and 4 (left panel) indicates the growing impact on the attenuation of X-rays within the collected PM, resulting in significant differences in the  $\overline{XSW}(\theta)$  between the different samples. The vertical bar in the left panel indicates the position typically selected for a TXRF measurement for a Si substrate and the incident photon energy used. This position was used for the calculation of  $\overline{XSW}(\theta)$  (Supp. Fig. 2).

Besides the differences in the XSW a further reason for the deviation in the quantification of the mass deposition at different incidence angles is that the full volume of the PM collected is not illuminated homogeneously in its depth direction because of the attenuation of the incident and reflected X-ray radiation. For increasing incidence angles and high surface coverage the effective path length is reduced as  $\frac{1}{\sin\theta}$  such that the X-ray attenuation within the PM volume becomes less pronounced. This argument becomes even more evident when considering that under conditions where an XSW is expected and for high surface density of PM, the photons need to travel twice through the airborne PM collected.

This insight impacts directly the reliability of TXRF quantification results in the sense

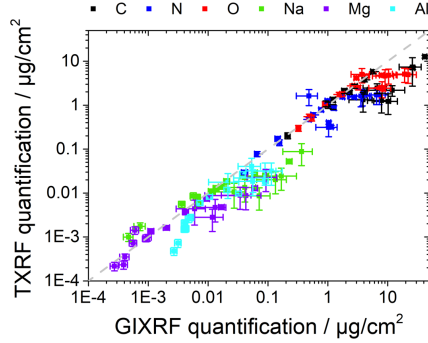


Figure 5: Comparison of the quantified mass deposition for TXRF and XRF (under shallow incidence angles). In the case of low mass depositions, the expected 1:1 ratio indicated by the dashed line is matched but for increasing mass deposition a deviation is observed which indicates that under TXRF conditions the quantified mass deposition underestimates the actually deposited mass deposition. This does not become apparent from the TXRF measurement itself. Therefore more exhaustive data as collected during a GIXRF measurement is required.

that TXRF underestimates the mass of PM collected for the samples with the highest loading which, in general, is due to exceedingly long collection times or high pollution levels. The strategy to collect by means of GIXRF more exhaustive data to quantify the mass deposition of the collected PM under different incidence angles and excitation conditions allows assessing the reliability and validity of the quantification performed. A self-consistent verification of the quantification can be performed by means of GIXRF by either having an agreement throughout the full angular range, i.e. with and without XSW, respectively virtually constant quantification results in case no XSW needs to be considered ( $\theta > 3\theta_c$ ). In the first case low mass depositions are investigated and the better sensitivity in terms of detection limit offered by TXRF can be profited from to perform quantification. In the second case, where deviations between GIXRF and TXRF quantification, are observed higher mass depositions are investigated. GIXRF allows nevertheless for robust and reliable quantification since in this angular regime the quantification is less prone to attenuation of the incident X-ray photons. Data at larger incidence angles where no XSW needs to be considered allows assessing the impact of X-ray attenuation within the airborne PM collected on the results. In view of the demands on quantitative techniques for regulatory purposes this critical assess-

ment of the validity of the results is mandatory. On a further positive note, the requirement for sufficiently low attenuation of X-rays, i.e., adequately short collection times of PM, for reliable TXRF quantification makes it mandatory to use effectively the sensitivity in terms of detection limits offered by TXRF and is beneficial for the time resolution which can be achieved during field campaigns.

For the extreme case of the two samples with the highest PM loads (panels E and F in Figs. 2 and 3) the variation of the quantified mass deposition with the incident angle indicates that an accurate quantification is tedious since here the attenuation of the incident radiation within the PM collected would need to be considered. This aspect introduces considerable uncertainties in the final result. Hence, a GIXRF measurement allows to discard these types of samples from further use in measurement campaigns.

When comparing for all 19 samples investigated the quantified mass deposition under TXRF conditions and when using the largest incidence angles such that no XSW is created, the deviation from the expected ratio with increasing elemental mass deposition becomes even more evident (Fig. 5). A better representation would be using the total mass, but due to the soft X-ray radiation used it can not be ascertained that the XRF radiation for all elements present in the matrix was excited. In general, this deviation indicates that for reliable quantification under TXRF conditions the attenuation of X-rays within the collected airborne PM and the differences in the XSW created should remain below a threshold value. This criteria cannot be specified generically since it depends on the incident photon energy and the absolute elemental composition of the PM. Hence for field campaigns where high-throughput TXRF quantification of PM collected on suitable substrates by means of laboratory instrumentation is conducted at least a subset of the samples should be investigated in more details. It has to be noted, that the GIXRF measurement can be restricted to few points since only data for an incidence angle typically chosen for a TXRF measurement and for a series of larger incidence angles ( $\theta > 3\theta_c$ ) is needed for cross-checking the quantification results.

In addition, simple control monitors can be used to identify possible issues with the quantification performed, regardless if standards are used or a reference-free quantification scheme is being applied. One indicator is the reflectivity from the substrate which can even be used when samples are investigated under TXRF conditions solely. An other indicator during a GIXRF measurement is that the X-ray radiation from the bulk volume of the substrate can be used to validate the quantification results (Supp. Fig. 3). For increasing mass deposition of airborne PM and larger incidence angles significant attenuation compared to a blank Si substrate can be observed. For both control monitors, a direct comparison to blank substrates (or calibration samples) allows elucidating if the amount of airborne PM collected might be too important for quantification by means of TXRF alone.

## Conclusion & Outlook

It was shown that GIXRF allows for applying robust quantification scheme and hence for assessing the validity of quantification under TXRF conditions. While increasing mass deposition results in different XSW created on the top of the substrates and pronounced attenuation of the incident and reflected X-rays within the airborne PM collected, the comparison of quantification results between TXRF and GIXRF for a subset of samples covering the full range of mass depositions of the airborne PM collected during a measurement campaign allows assessing the limits for reliable quantification results and identifying the range of samples where quantification should be realized by means of GIXRF. This information on the validity of the quantification results depends on the matrix composition and the incident photon energy, but cannot be assessed from TXRF measurements alone. It has to be noted that the presented experiment with its emphasis on light elements was realized in the soft X-ray regime but the conclusions made can also be applied for higher X-ray energies.

While advanced instrumentation was applied for allowing for a physically traceable quantification which does not rely on the use of standards, it can be emphasized that this approach

is transferable to laboratory instrumentation.<sup>49</sup> Indeed, manufacturers of TXRF instrumentation start offering advanced instrumentation where the incidence angle of the monochromatized exciting radiation can be tuned. Thus, possibilities are offered to transfer the approach presented to instrumentation used for high-throughput measurements in the field or in the laboratory. Even without tuning the incident angle the implementation of a diode to measure the reflectivity would allow a rough but straightforward indication whether the quantity of airborne PM collected presents an issue for the quantification by means of TXRF. Furthermore, differences in the XSW between samples with different quantities of airborne PM could be accounted for.

## **Acknowledgement**

Parts of this research was performed within the EMPIR project 19ENV08 AEROMET II. This project has received funding from the EMPIR programme co-financed by the Participating States and from the European Union's Horizon 2020 research and innovation programme. The support of the European Structural and Investment Funds jointly financed by the European Commission and the Hungarian Government through grant no. VEKOP-2.3.2-16-2016-00011 (on behalf of J. Osán) is also appreciated.

## References

- (1) Apte, J. S.; Marshall, J. D.; Cohen, A. J.; Brauer, M. Addressing Global Mortality from Ambient PM<sub>2.5</sub>. *Environ. Sci. Technol.* **2015**, *49*, 8057–8066.
- (2) Lelieveld, J.; Evans, J. S.; Fnais, M.; Giannadaki, D.; Pozzer, A. The contribution of outdoor air pollution sources to premature mortality on a global scale. *Nature* **2015**, *525*, 367–371.
- (3) Leni, Z.; Cassagnes, L. E.; Daellenbach, K. R.; El Haddad, I.; Vlachou, A.; Uzu, G.; Prévôt, A. S. H.; Jaffrezo, J.-L.; Baumlin, N.; Salathe, M.; Baltensperger, U.; Dommen, J.; Geiser, M. Oxidative stress-induced inflammation in susceptible airways by anthropogenic aerosol. *PLOS ONE* **2020**, *15*, 1–17.
- (4) Mellouki, A.; Wallington, T. J.; Chen, J. Atmospheric Chemistry of Oxygenated Volatile Organic Compounds: Impacts on Air Quality and Climate. *Chem. Rev.* **2015**, *115*, 3984–4014.
- (5) McNeill, V. F. Aqueous Organic Chemistry in the Atmosphere: Sources and Chemical Processing of Organic Aerosols. *Environ. Sci. Technol.* **2015**, *49*, 1237–1244.
- (6) Zhang, R.; Wang, G.; Guo, S.; Zamora, M. L.; Ying, Q.; Lin, Y.; Wang, W.; Hu, M.; Wang, Y. Formation of Urban Fine Particulate Matter. *Chem. Rev.* **2015**, *115*, 3803 – 3855.
- (7) Prather, K. A.; Hatch, C. D.; Grassian, V. H. Analysis of Atmospheric Aerosols. *Annu. Rev. Anal. Chem.* **2008**, *1*, 485–514.
- (8) Møller, P.; Folkmann, J. K.; Forchhammer, L.; Bräuner, E. V.; Danielsen, P. H.; Risom, L.; Loft, S. Air pollution, oxidative damage to DNA, and carcinogenesis. *Cancer Lett.* **2008**, *266*, 84 – 97.

- (9) Stone, V.; Johnston, H.; Clift, M. J. D. Air Pollution, Ultrafine and Nanoparticle Toxicology: Cellular and Molecular Interactions. *IEEE Transactions on NanoBioscience* **2007**, *6*, 331–340.
- (10) Valavanidis, A.; Fiotakis, K.; Vlachogianni, T. Airborne Particulate Matter and Human Health: Toxicological Assessment and Importance of Size and Composition of Particles for Oxidative Damage and Carcinogenic Mechanisms. *J. Environ. Sci. Health Pt. C* **2008**, *26*, 339–362.
- (11) Brook, R. D.; Rajagopalan, S.; Pope, C. A.; Brook, J. R.; Bhatnagar, A.; Diez-Roux, A. V.; Holguin, F.; Hong, Y.; Luepker, R. V.; Mittleman, M. A.; Peters, A.; Siscovick, D.; Smith, S. C.; Whitsel, L.; Kaufman, J. D. Particulate Matter Air Pollution and Cardiovascular Disease. *Circulation* **2010**, *121*, 2331–2378.
- (12) Rönkkö, T.; Timonen, H. Overview of Sources and Characteristics of Nanoparticles in Urban Traffic-Influenced Areas. *J Alzheimers Dis.* **2019**, *72*, 15–28.
- (13) Daellenbach, K. R. et al. Sources of particulate-matter air pollution and its oxidative potential in Europe. *Nature* **2020**, *587*, 414–419.
- (14) Bulska, E.; Ruszczyńska, A. Analytical Techniques for Trace Element Determination. *Phys. Sci. Rev.* **2017**, *2*, 20178002.
- (15) Ault, A. P.; Axson, J. L. Atmospheric Aerosol Chemistry: Spectroscopic and Microscopic Advances. *Anal. Chem.* **2017**, *89*, 430–452, PMID: 28105816.
- (16) Furger, M.; Minguillón, M. C.; Yadav, V.; Slowik, J. G.; Hüglin, C.; Fröhlich, R.; Petterson, K.; Baltensperger, U.; Prévôt, A. S. H. Elemental composition of ambient aerosols measured with high temporal resolution using an online XRF spectrometer. *Atmos. Meas. Tech.* **2017**, *10*, 2061–2076.

- (17) Bukowiecki, N.; Lienemann, P.; Zwicky, C. N.; Furger, M.; Richard, A.; Falkenberg, G.; Rickers, K.; Grolimund, D.; Borca, C.; Hill, M.; Gehrig, R.; Baltensperger, U. X-ray fluorescence spectrometry for high throughput analysis of atmospheric aerosol samples: The benefits of synchrotron X-rays. *Spectrochim. Acta B* **2008**, *63*, 929 – 938.
- (18) Richard, A.; Bukowiecki, N.; Lienemann, P.; Furger, M.; Fierz, M.; Minguillón, M. C.; Weideli, B.; Figi, R.; Flechsig, U.; Appel, K.; Prévôt, A. S. H.; Baltensperger, U. Quantitative sampling and analysis of trace elements in atmospheric aerosols: impactor characterization and Synchrotron-XRF mass calibration. *Atmos. Meas. Tech.* **2010**, *3*, 1473–1485.
- (19) Klockenkämper, R.; Bayer, H.; von Bohlen, A.; Schmeling, M.; Klockow, D. Collection of Airborne Particulate Matter for a Subsequent Analysis by Total Reflection X-Ray Fluorescence. *Anal. Sci.* **1995**, *11*, 495–498.
- (20) Bontempi, E.; Zacco, A.; Benedetti, D.; Borgese, L.; Colombi, P.; Stosnach, H.; Finzi, G.; Apostoli, P.; Buttini, P.; Depero, L. Total reflection X-ray fluorescence (TXRF) for direct analysis of aerosol particle samples. *Environ. Technol.* **2010**, *31*, 467–477.
- (21) Prost, J.; Wobrauschek, P.; Strel, C. Quantitative total reflection X-ray fluorescence analysis of directly collected aerosol samples. *X-Ray Spectrom.* **2017**, *46*, 454–460.
- (22) Osán, J.; Börcsök, E.; Czömpöly, O.; Dian, C.; Groma, V.; Stabile, L.; Török, S. Experimental evaluation of the in-the-field capabilities of total-reflection X-ray fluorescence analysis to trace fine and ultrafine aerosol particles in populated areas. *Spectrochim. Acta B* **2020**, *167*, 105852.
- (23) Fomba, K. W.; Deabji, N.; Barcha, S. E. I.; Ouchen, I.; Elbaramoussi, E. M.; El Moursli, R. C.; Harnafi, M.; El Hajjaji, S.; Mellouki, A.; Herrmann, H. Application

- of TXRF in monitoring trace metals in particulate matter and cloud water. *Atmos. Meas. Tech.* **2020**, *13*, 4773–4790.
- (24) Bukowiecki, N.; Hill, M.; Gehrig, R.; Zwicky, C. N.; Lienemann, P.; Hegedüs, F.; Falkenberg, G.; Weingartner, E.; Baltensperger, U. Trace Metals in Ambient Air: Hourly Size-Segregated Mass Concentrations Determined by Synchrotron-XRF. *Environ. Sci. Technol.* **2005**, *39*, 5754–5762.
- (25) Beckhoff, B.; Fliegau, R.; Kolbe, M.; Müller, M.; Weser, J.; Ulm, G. Reference-Free Total Reflection X-ray Fluorescence Analysis of Semiconductor Surfaces with Synchrotron Radiation. *Anal. Chem.* **2007**, *79*, 7873–7882.
- (26) Strel, C.; Wobrauschek, P.; Meirer, F.; Pepponi, G. Synchrotron radiation induced TXRF. *J. Anal. At. Spectrom.* **2008**, *23*, 792–798.
- (27) Borgese, L.; Bilo, F.; Zacco, A.; Federici, S.; Mutahi, A. W.; Bontempi, E.; Trzepla, K.; Hyslop, N.; Yatkin, S.; Wobrauschek, P.; Prost, J.; Ingerle, D.; Depero, L. E. The assessment of a method for measurements and lead quantification in air particulate matter using total reflection X-ray fluorescence spectrometers. *Spectrochim. Acta B* **2020**, *167*, 105840.
- (28) Klockenkämper, R.; von Bohlen, A. *Total Reflection X-Ray Fluorescence Analysis and Related Methods*; John Wiley & Sons, Ltd, 2014.
- (29) Hönicke, P.; Krämer, M.; Lühl, L.; Andrianov, K.; Beckhoff, B.; Dietsch, R.; Holz, T.; Kanngießner, B.; Weißbach, D.; Wilhein, T. Development and characterization of sub-monolayer coatings as novel calibration samples for X-ray spectroscopy. *Spectrochim. Acta B* **2018**, *145*, 36 – 42.
- (30) Horntrich, C.; Kregsamer, P.; Prost, J.; Stadlbauer, F.; Wobrauschek, P.; Strel, C. Production of the ideal sample shape for Total Reflection X-ray Fluorescence analysis. *Spectrochim. Acta B* **2012**, *77*, 31 – 34.

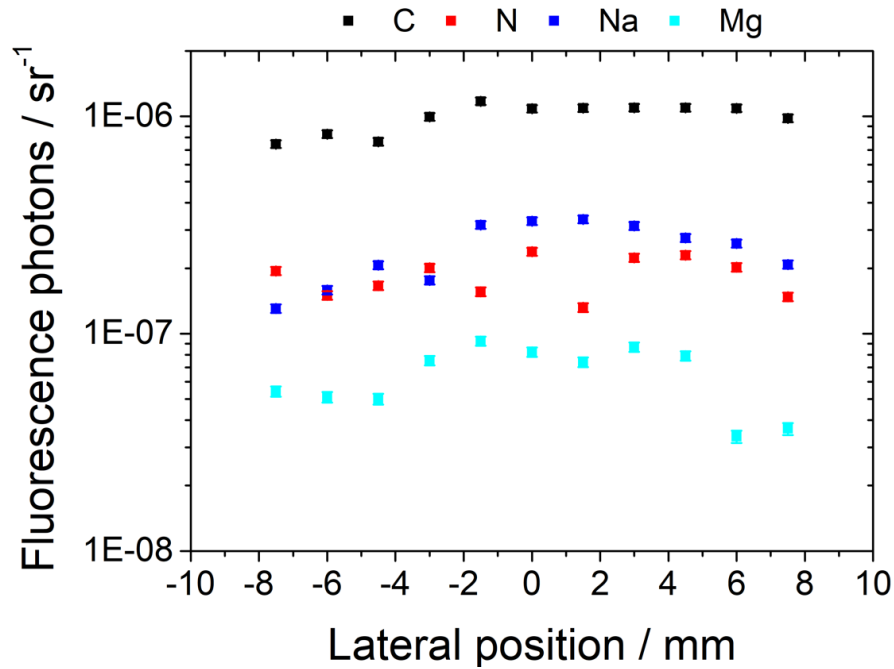
- (31) Böttger, S.; Tyssebotn, I. M. B.; Jansen, W.; Fittschen, U. E. Evaluating internal standards for the determination of gas phase mercury using silver nanoparticle assisted total reflection X-ray fluorescence. *Spectrochim. Acta B* **2018**, *147*, 93 – 99.
- (32) May, K. An “ultimate” cascade impactor for aerosol assessment. *J. Aerosol Sci.* **1975**, *6*, 413 – 419.
- (33) Marple, V. A. History of Impactors—The First 110 Years. *Aerosol Sci. Technol.* **2004**, *38*, 247–292.
- (34) Müller, M.; Hönicke, P.; Detlefs, B.; Fleischmann, C. Characterization of High-k Nanolayers by Grazing Incidence X-ray Spectrometry. *Materials* **2014**, *7*, 3147–3159.
- (35) Hönicke, P.; Detlefs, B.; Nolot, E.; Kayser, Y.; Mühle, U.; Pollakowski, B.; Beckhoff, B. Reference-free grazing incidence x-ray fluorescence and reflectometry as a methodology for independent validation of x-ray reflectometry on ultrathin layer stacks and a depth-dependent characterization. *Journal of Vacuum Science & Technology A* **2019**, *37*, 041502.
- (36) Senf, F.; Flechsig, U.; Eggenstein, F.; Gudat, W.; Klein, R.; Rabus, H.; Ulm, G. A plane-grating monochromator beamline for the PTB undulators at BESSY II. *Journal of Synchrotron Radiation* **1998**, *5*, 780–782.
- (37) Lubeck, J.; Beckhoff, B.; Fliegau, R.; Holfelder, I.; Hönicke, P.; Müller, M.; Pollakowski, B.; Reinhardt, F.; Weser, J. A novel instrument for quantitative nanoanalytics involving complementary X-ray methodologies. *Rev. Sci. Instrum.* **2013**, *84*, 045106.
- (38) Scholze, F.; Procop, M. Modelling the response function of energy dispersive X-ray spectrometers with silicon detectors. *X-Ray Spectrom.* **2009**, *38*, 312–321.
- (39) Scholze, F.; Procop, M. Detection efficiency of energy-dispersive detectors with low-energy windows. *X-Ray Spectrom.* **2005**, *34*, 473–476.

- (40) Müller, M.; Beckhoff, B.; Ulm, G.; Kanngießner, B. Absolute determination of cross sections for resonant Raman scattering on silicon. *Phys. Rev. A* **2006**, *74*, 012702.
- (41) Unterumsberger, R.; Hönicke, P.; Kayser, Y.; Pollakowski-Herrmann, B.; Gholhaki, S.; Guo, Q.; Palmer, R. E.; Beckhoff, B. Interaction of nanoparticle properties and X-ray analytical techniques. *J. Anal. At. Spectrom.* **2020**, *35*, 1022–1033.
- (42) Kayser, Y.; Sá, J.; Szlachetko, J. Nanoparticle characterization by means of scanning free grazing emission X-ray fluorescence. *Nanoscale* **2015**, *7*, 9320–9330.
- (43) Schoonjans, T.; Brunetti, A.; Golosio, B.; Sanchez del Rio, M.; Solé, V. A.; Ferrero, C.; Vincze, L. The xraylib library for X-ray–matter interactions. Recent developments. *Spectrochim. Acta B* **2011**, *66*, 776 – 784.
- (44) Beckhoff, B.; Ulm, G.; Bundesanstalt, P.-T. Determination of fluorescence yields using monochromized undulator radiation of high spectral purity and well known flux. *Adv. X-Ray Anal.* **2001**, *44*, 349–354.
- (45) Hönicke, P.; Kolbe, M.; Krumrey, M.; Unterumsberger, R.; Beckhoff, B. Experimental determination of the oxygen K-shell fluorescence yield using thin SiO<sub>2</sub> and Al<sub>2</sub>O<sub>3</sub> foils. *Spectrochim. Acta B* **2016**, *124*, 94 – 98.
- (46) Wählich, A.; Streeck, C.; Hönicke, P.; Beckhoff, B. Validation of secondary fluorescence excitation in quantitative X-ray fluorescence analysis of thin alloy films. *J. Anal. At. Spectrom.* **2020**, *35*, 1664–1670.
- (47) Klockenkämper, R.; von Bohlen, A. Determination of the critical thickness and the sensitivity for thin-film analysis by total reflection X-ray fluorescence spectrometry. *Spectrochim. Acta B* **1989**, *44*, 461 – 469.
- (48) Hellin, D.; Fyen, W.; Rip, J.; Delande, T.; Mertens, P. W.; De Gendt, S.; Vinckier, C.

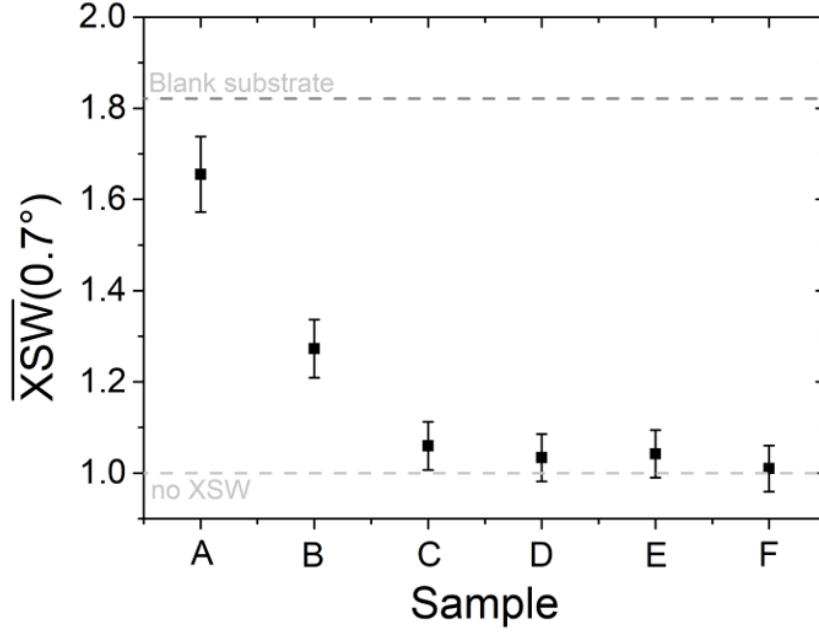
Saturation effects in TXRF on micro-droplet residue samples. *J. Anal. At. Spectrom.* **2004**, *19*, 1517–1523.

- (49) Hönicke, P.; Waldschläger, U.; Wiesner, T.; Krämer, M.; Beckhoff, B. Towards a calibration of laboratory setups for grazing incidence and total-reflection X-ray fluorescence analysis. *Spectrochim. Acta B* **2020**, *174*, 106009.

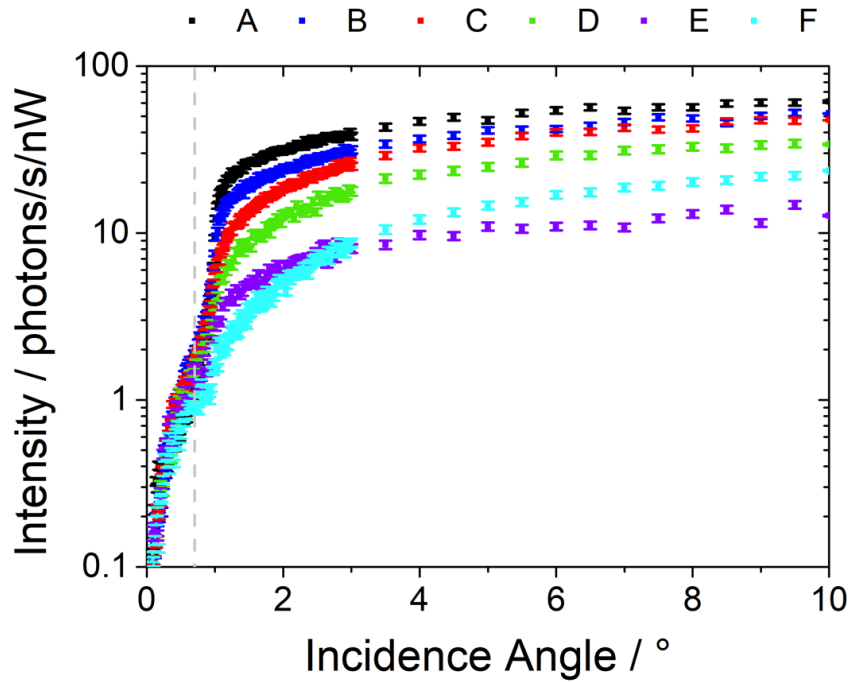
Supplementary information - Peculiarities in quantification of airborne particulate matter by means of Total Reflection X-ray Fluorescence



Supp. Fig. 1: Lateral scan along the line of the deposition pattern exhibiting that in the central area a quite uniform distribution has been achieved. Due to the shallow incidence angle of  $5^\circ$ , the position close to the boarder of the sample could not be investigated but no decreased collection efficiency is expected from design consideration of the May-type cascade impactor. The sample is the one for which the GIXRF data is displayed in Fig. 1.



Supp. Fig. 2: An increasing mass deposition affects the contrast in optical density at the interface defined by the surface of the substrate: while for a low mass deposition the surface coverage is low enough to assume that the airborne PM does not alter the optical properties in the area above the substrate surface, this assumption does not hold for high mass deposition and the optical properties of the airborne PM for the incident X-ray radiation needs to be considered in addition to optical properties of the substrate. based on the measured reflectivity at an incidence angle of  $0.7^\circ$  (as shown in Fig. 4, vertical bar), significant differences in the  $\overline{XSW}(\theta)$  between the different samples are obtained. The horizontal bars indicate the relative XSW factor which can be expected from the reflectivity measured from a blank Si substrate without PM on the top of it, respectively in the case no XSW is present because the reflectivity has dropped to 0. Finally, the measured reflectivity can be used as a monitor for assessing whether comparable excitation conditions are achieved for a sample set under investigation.



Supp. Fig. 3: The detected Si XRF fluorescence originating from the L-shell for the same samples than displayed in Figures 2 and 4 indicate the growing impact on the attenuation of X-rays within the collected PM. The vertical bar indicates the position typically selected for a TXRF measurement for a Si substrate and the incident photon energy used. In contrast to the reflectivity (Fig. 4) which can be used as an indicator for exceedingly high mass deposition with respect to a reliable quantification of the mass deposition by means of TXRF, scattering or fluorescence signals from the bulk substrate can be used more conveniently as monitors during GIXRF measurements in the range above the critical angle of total external reflection. In both cases, reflectivity and XRF from the bulk substrate, a simple cross-comparison to a blank substrate will be sufficient.